

**Figure 8.** Possible arrangement of the two-meter long prototype coil T0 in combination with a cold iron yoke to generate the windings internal stress and force levels as in the full size detector toroid.

• and finally the performance test of the coil.

Ideally, during the test of the single shorter T0 coil the actual stress and Lorentz forces per meter as present in the full size toroid coil windings should be approximated in order to qualify the mechanical soundness of the coil windings and check its vulnerability for training. This can be achieved by testing the prototype coil at an excess operating current, eventually in combination with a cold-iron mirror temporarily attached to the test coil for this purpose. A test setup of the T0 coil adapted to the constraints of the test facility is shown in figure 8. With iron present this arrangement can produce the 50 MPa coil windings stress as in the full toroid at a test current of 14.9 kA (excess of 2.6 kA) and a peak magnetic field of 5.5 T. The pulling force on the straight section of the coil is then some 0.45 MN/m. Without iron a test current of 16.2 kA (excess of 3.9 kA) is needed for generating 50 MPa with 5.6 T peak magnetic field. However, in this case there is no pulling force on the coil inner beam.

## 3 The IAXO x-ray optics

#### 3.1 Basic considerations

The purpose of the x-ray optics is to focus the putative x-ray signal to as small a spot as possible, and in doing so, reduce the size of the detector required and, ultimately, the detector background. The performance of an x-ray optic is generally characterized by three basic properties: the point spread function (PSF), the shape of the resultant spot; the throughput,  $\epsilon_o$ , the amount of incident photons properly focused by the optic; and the field-of-view (FOV), the extent to which the optic can focus off-axis photons.

Although x-ray optics can rely on refraction, diffraction or reflection, the large entrance pupil and energy band required for IAXO lead us to only consider grazing-incidence reflective optics. To achieve the smallest spot a, the optics should have as short a focal length, f, as possible since the spot area grows quadratically with focal length,  $a \propto f^2$ . At the same time, the individual mirrors that comprise the optic should have the highest x-ray reflectivity. Reflectivity increases with decreasing

graze angle,  $\alpha$ , and since  $f \propto \frac{1}{\alpha}$ , to achieve the highest throughput the optics should have as long a focal length as possible.

Further complicating the optical design is that the  $\epsilon_o$ , FOV and PSF of an optic have a complex dependence on the the incident photon energy E and  $\alpha$ .

- **Throughput:** there are many choices for the coatings of an x-ray mirror. These coatings can have abrupt changes in reflectivity as a function of energy when the pass-band includes the characteristic absorption edges of the constituent materials. And as already discussed, the reflectivity will be higher with decreasing graze angle.
- **Field-of-view:** the FOV is impacted by a phenomenon referred to a "vignetting," the loss of photons that pass through the entrance aperture of the optic but are not properly focused on the focal plane. Vignetting is more severe at lower graze angles and increases with the off-axis position. Vignetting is a geometric effect and would occur even if the coatings have 100% reflectivity. When realistic coatings, with their own dependence on *E*, are accounted for, the FOV becomes dependent on the photon energy and decreases at higher energies.
- **Point Spread Function:** the PSF of an x-ray telescope depends on several factors including the basic design, the long spatial frequency errors (usually referred to as figure errors) and short spatial frequency errors (usually refereed to as finish errors). These first two factors can be accounted for using geometric optics treatments and do not have a formal energy dependence. But like the FOV, once realistic coatings are considered, the PSF can take on a mild energy dependence. Finish errors can be accounted for using wave optics treatments (e.g., scattering theory) that depend on both E and  $\alpha$ . Several authors have shown that the transition between the valid use of geometric and wave optics itself has a dependence on E and  $\alpha$ , so the final energy dependence of the PSF is not easily described by a simple relationship.

There are two basic families of reflective x-ray optics: those that employ two reflections to (nearly) satisfy the Abbe sine rule and have excellent imaging properties across its FOV; those that employ a single reflection and have poor imaging properties. The former include a family of designs originally proposed by Wolter and include telescopes and point-to-point imagers; the later include concentrators and collimators.

Since the x-rays produced via the conversion of axions to photons in the IAXO magnet have the same directionality of the axions, the optic need only have a FOV slightly larger than the inner 3 arcminute ( $\sim$ 0.9 mrad) Solar disk, the region of axion production. Moreover, the fact the emission is from a uniformly filled extended region means that, to first order, a telescope or concentrator with the same focal length f will result in the same focused spot of  $\sim$  1.0  $\times$   $f_{\rm m}$  mm, where  $f_{\rm m}$  is the focal length in meters. The focal length of the optic, be it a collimator or a telescope, depends on the radius of the largest shell and maximum graze angle that can still result in a high reflectivity from the mirror shell. For a telescope, the relationship is  $f \propto \frac{\rho_{\rm max}}{4\alpha}$ , while for a collimator it is  $f \propto \frac{\rho_{\rm max}}{2\alpha}$ .

To zeroth order, the x-ray reflectivity at a single energy of a single metal film is near-unity up to a certain angle, called the critical angle, and then zero above that angle. If this were strictly true, a telescope would be the clear winning design for IAXO, since it would have half the focal length, and hence half the spot diameter and one-fourth the area of a collimator.

However, we know that the reflectivity in the  $1-10 \,\mathrm{keV}$  has a more complex relationship as a function of energy and  $\alpha$ . The throughput of the optics will depend on the reflectivity, which in turn depends on the coating material and graze angle, and the optical design, which determines the number of reflections a photon will experience as it passes through the optic: for a collimator, n=1 while for a telescope, n=2.

#### 3.2 Fabrication techniques for reflective optics

The x-ray astronomy community has designed, built and flown x-ray telescopes on more than ten satellite missions, and they have developed a number of techniques for fabricating the telescopes. For each technology, we give a brief description and cite examples of telescopes that rely on it. Broadly speaking, telescopes can be classed into two groups that depend on how they are assembled. Segmented optics rely on several individual pieces of substrates to complete a single layer. (The appropriate analogy is the way a barrel is assembled from many individual staves.) Integral-shell optics are just that: the hyperbolic or parabolic shell is a single monolithic piece.

### 3.2.1 Segmented optics: rolled aluminum substrates

Telescopes formed from segmented aluminum substrates were first utilized for the broad band x-ray telescope (BBXRT) that flew on the Space Shuttle in 1990 [38]. Later missions that used the same approach included: *ASCA* [39], launched in 1993; SODART [40], completed in 1995 but never launched; InFocµs [41], a hard x-ray balloon-borne instrument flown in 2004; and *Suzaku* [42], launched in 2005. Aluminum substrates will also be used for the soft and hard X-ray telescopes on the upcoming JAXA Astro-H (also called NeXT) mission, scheduled for launch in 2014 [43].

#### 3.2.2 Segmented optics: glass substrates

Although using glass substrates for an x-ray telescope was explored as far as back as the 1980s [44], it was not fully realized until 2005 with the launch of HEFT [45]. HEFT had three, hard x-ray telescopes, each consisting of as many as 72 layers. HEFT was the pathfinder for NASA's *NuS-TAR* [46], launched in 2012 and the first satellite mission to use focusing x-ray optics to image in the hard x-ray band up to 80 keV. Each of *NuSTAR's* two telescope consists of 130 layers, comprised of more than 2300 multilayer-coated pieces of glass. Finally, slumped glass is a candidate technology being developed by several groups for future NASA and ESA missions, like ATHENA (see, e.g., [47] and [48]).

## 3.2.3 Segmented optics: silicon substrates

Another technology being pursued for ATHENA are silicon pore optics [49], which consists of silicon wafers that have a reflective coating on one side and etched support structures on the other. Individual segments are stacked on top of each other to build nested layers. Prototype optics have been built and tested, but there are no operational x-ray telescope yet to use this method.

# 3.2.4 Integral shell optics: replication

Replicated optics are created by growing the mirror, usually a nickel-based alloy, on top of a precisely figured and polished mandrel or master. The completely-formed shell is separated from the

mandrel, and two unique mandrels are required for each individual layer (one for the parabolic-shaped primary, another for the hyperbolic-shaped secondary). Missions that have utilized replicated x-ray telescopes include: *XMM* [50], launched in 1999; *Beppo-SAX* [51], launched in 1996; *ABRIXAS* [52], launched in 1999; the balloon-borne HERO mission [53], first flown in 2002; and the sounding rocket mission FOXSI, currently under development. It is important to mention that CAST currently employs a flight-spare telescope from *ABRIXAS*.

## 3.2.5 Integral shell optics: monolithic glass

For completeness, we mention telescopes formed from monolithic pieces of glass. Although these telescopes have excellent focusing quality and have produced some of the best images of the x-ray sky, because of the cost and weight, no future mission is expected to use this approach. Missions that have utilized monolithic optics include: *Einstein* [54], launched in (1978); *RoSAT*, [55] launched in 1980; and the *Chandra X-ray Observatory* [56], launched in 1998.

## 3.3 The baseline technology for IAXO

For IAXO, we have adopted segmented, slumped glass optics as the baseline fabrication approach for several reasons. First, the technology is mature and has been developed by members of the IAXO collaboration, most recently for the NuSTAR satellite mission. Second, this approach easily facilitates the deposition of single-layer or multi-layer reflective coatings. Third, it is the least expensive of the fabrication techniques. Fourth, the imaging requirement for solar observations for IAXO is very modest-focusing the central 3 arcminute core of the Sun. Although other optics technologies may have better resolution than slumped glass, they would not produce a significantly smaller focused spot of the solar core.

# 3.4 The IAXO x-ray telescopes

#### 3.4.1 Design and optimization of the IAXO x-ray telescopes

The optical prescription and reflective coatings were identified by a systematic search of a multidimensional parameter space that accounted for the detector efficiency, axion spectrum, optics properties and recipe of the reflective coatings. The total optics and detector figure of merit,  $f_{DO}$  was then computed. The optical prescription and multilayer recipes presented below produced the highest  $f_{DO}$ . It is important to note that the telescope optimization *must* account for the axion spectrum and detector efficiency and cannot be performed independently. If this process does not include these energy dependent terms,  $f_{DO}$  will not achieve the highest possible value.

Telescope prescriptions were generated for designs that had a fixed maximum radius of 300 mm and a minimum radius of 50 mm, with the focal length varied between 4 and 10 m, in increments of 1 m. As the focal length is increased and the graze angle,  $\alpha$ , decreases and the number of nested layers increases. For example, the f=4 m design has 110 nested layers, while the f=10 m design has more than 230 layers.

Traditionally, x-ray telescopes have relied on single layer coatings of metals like Au or Ir to achieve high throughput in the  $1-10\,\text{keV}$  band. More recently, missions designed for hard x-ray observations, like NuSTAR and ASTRO-H, have employed multilayer coatings to achieve high reflectivity up to  $\sim\!80\,\text{keV}$ . We explored combinations of both for IAXO. Although it is theoretically

possible to optimize the coating for each layer of the telescope, this would impose a high penalty in resources when depositing multilayers on the substrates. Instead, we divided the layers into ten sub-groups, with each sub-group of layers receiving the same multilayer coating. A similar strategy was successfully implemented for NuSTAR [57], and this approach allowed the multilayer deposition tools to be used efficiently.

Material types investigated were single layers of W and W/B<sub>4</sub>C multilayers. Other types/combinations to consider are W/Si, Pt/B<sub>4</sub>C, Ir/B<sub>4</sub>C and Ni/B<sub>4</sub>C. W/B<sub>4</sub>C and W/Si are well understood coatings for x-ray reflectivity and considerably less expensive to use W than Pt or Ir. Using B<sub>4</sub>C instead of Si as the light material will give increasedF reflectivity at 1–4 keV, but also gives slightly higher stress in the coating. Ni/B<sub>4</sub>C coatings are not well understood and can give a high interfacial roughness between light and heavy material, but performs similar to W/B<sub>4</sub>C and Ir/B<sub>4</sub>C at 1–10 keV.

At a given substrate incident angle,  $\alpha$ , the coating geometry was optimized by trying every combination in a parameter space of n (number of bilayers),  $d_{\min}$  (minimum bilayer thickness),  $d_{\max}$  (maximum bilayer thickness) and  $\Gamma$ , the ratio between the thickness of the heavy material with respect to the total thickness of the bilayer. For every combination, the x-ray reflectivity was calculated using IMD [58]. One of the basic properties of any x-ray telescope is the effective area, EA, the energy-dependent effective aperture of the telescope that accounts for finite reflectivity of individual mirror elements and physical obscuration present in the telescope (e.g., from the support structures used to fabricate the optics and the finite thickness of the substrate which absorbs incoming photons). The effective area of an individual layer i is given by:

$$EA(E)_i = GA_i \times R_i(E, \alpha)^2 \times 0.8,$$
(3.1)

where  $GA_i$  is the projected geometric area of the individual layer i,  $R_i(E, \alpha)$  is the reflectivity of the coatings on layer i and the constant factor of 0.8 accounts for obscuration. The total area is given by:

$$EA(E) = \sum_{i=1}^{N} EA_i(E), \qquad (3.2)$$

where N is the total number of layers. Figure 9 shows the expected behavior of the effective area increasing as the focal length grows. Again, this behavior arises from the fact that longer focal lengths results in shallower incident angles, and reflectivity increases with decreasing graze angles.

The energy-dependent optics throughput or efficiency,  $\epsilon_o(E)$ , is simply the EA(E) divided by the geometric area of the entrance pupil:

$$\epsilon_o(E) = \frac{\text{EA}(E)[\text{m}^2]}{\pi (0.3^2 - 0.05^2)[\text{m}^2]}.$$
(3.3)

The plot of figure 9 displays this quantity for different focal lengths.

In order to build a meaningful figure or merit we multiply the optics throughput by the energy-dependent axion flux  $\frac{d\phi}{dE}(E)$  expected from Primakoff production at the Sun [32] and the detector efficiency  $\epsilon_d(E)$ . The resulting quantity, that we call "detected axion flux" (DAF(E)),

$$DAF(E) = \sum_{i=1}^{N} EA_i(E) \times \epsilon_d(E) \times \frac{d\phi}{dE}(E)$$
(3.4)

is actually proportional to a hypothetical axion signal in IAXO, and is plotted in figure 10.

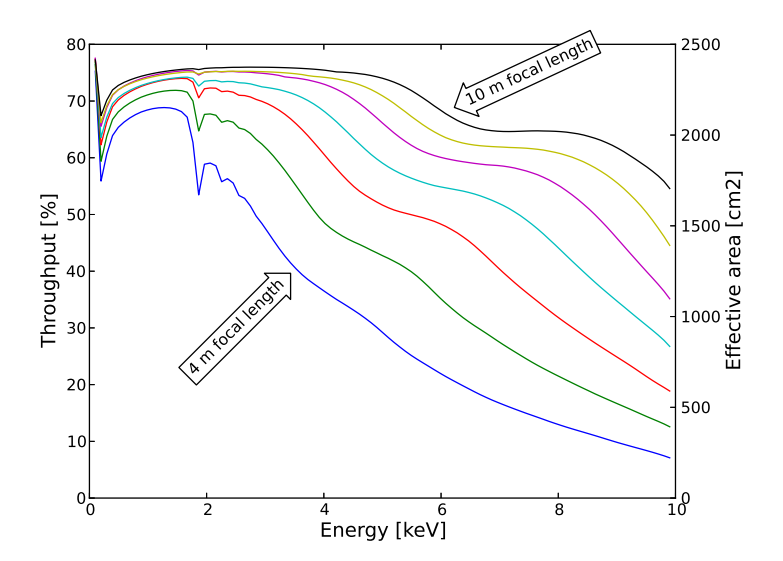


**Figure 9.** Effective area (right axis) and throughput/efficiency (left axis) versus photon energy for a single telescope for different focal lengths considered, from f = 4 m (lowest curve) up to f = 10 m (highest curve). Effective area grows as the focal length is increased.

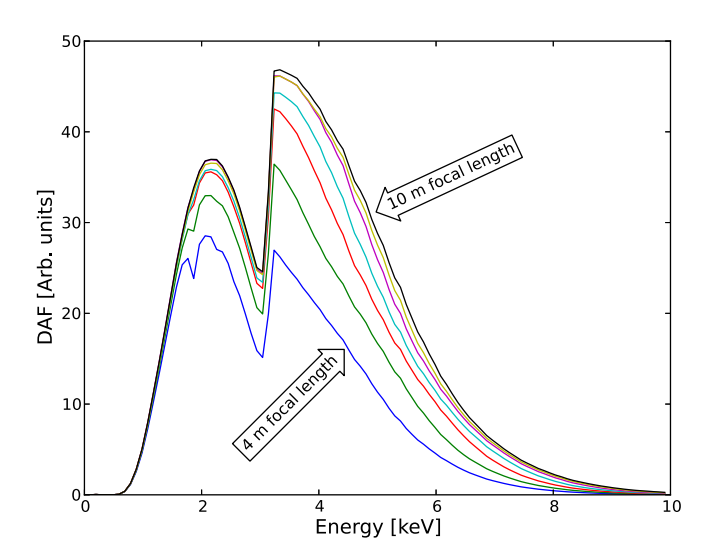


Figure 10. DAF versus photon energy E for a single telescope, and for the different focal lengths considered, from f = 4 m (lowest curve) up to f = 10 m (highest curve). The significant structure now present is due to absorption edges in detector and coating materials and the shape of the solar axion spectrum.

To find the optimal focal length, we need to maximize the integral of the DAF from 1–10 keV divided by the square root of the spot size (one could see this as the contribution from the optics to the figure of merit  $f_{DO}$  as defined in [32]):

$$f_O \equiv \int_{E=1 \,\text{keV}}^{10,\text{keV}} \left(\frac{\text{DAF}(E)}{\sqrt{a}}\right) dE.$$
 (3.5)

The only quantity left to compute is the spot-size, a. The point-spread-function (PSF) of any x-ray telescope has a complex shape, and the spot-size is computed by first taking the integral of the PSF to compute the encircled energy function (EEF), a measure of how much focused x-ray light is contained within the diameter of a particular size. For example, a common measure of the focusing quality of an x-ray telescope is to determine the 50% value of the EEF, that is to determine the smallest diameter extraction region that contains 50% of the power. This is often referred to as the half-power diameter or HPD.

The spot-size will depend on both the physical size of the object imaged, in this case the 3 arcminute (0.87 mrad) central core of the Sun, and the intrinsic imaging capability of the x-ray optic, i.e. the size of the resultant spot when the telescope images a point-like source. To first order, then, the overall spot size  $s_{\text{total}}$ , measured in angular extent, will be the root mean square of the object size  $s_{\text{obj}}$  and the optic quality  $s_{\text{opt}}$ :

$$s_{\text{total}} = \sqrt{s_{\text{obj}}^2 + s_{\text{opt}}^2}. \tag{3.6}$$

Based on the performance of the NuSTAR x-ray telescopes [46], we assume for the nominal design of the telescopes a HPD of 1 arcmin (0.29 mrad) and an 80% EEF of 2 arcmin (0.58 mrad). The angular spot size then becomes:

$$s_{\text{total}} = \sqrt{s_{\text{obj}}^2 + s_{\text{opt}}^2} = \sqrt{0.87^2 + 0.58^2} = 1.0 \,\text{mrad}.$$
 (3.7)

As discussed above, the spatial diameter of the spot is simply  $f \times s_{\text{total}}$  and the spot area becomes:

$$a = \frac{\pi}{4} \left( s_{\text{total}} \times f \right)^2. \tag{3.8}$$

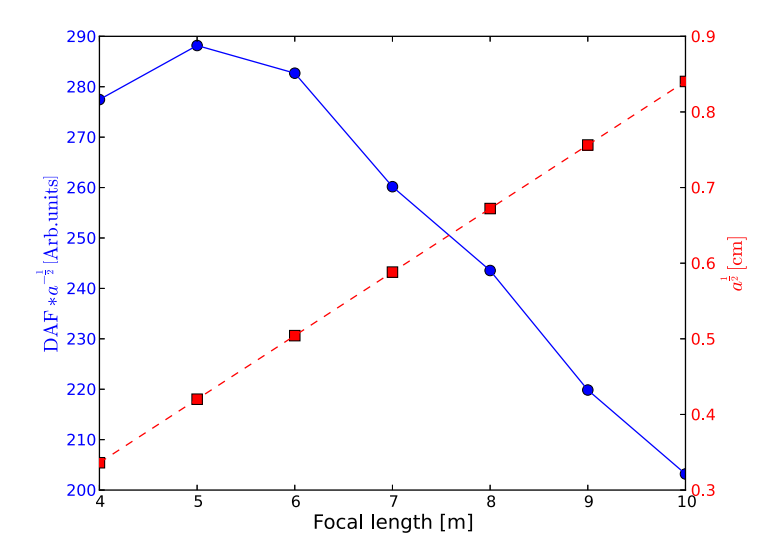
#### 3.4.2 Properties of the IAXO x-ray telescopes

Figure 11 shows  $\sqrt{a}$  as well as  $f_O$ , as calculated in eq. (3.5), as function of the focal length. The optimal focal length is found to be  $f=5\,\mathrm{m}$ . This parameter and the considerations exposed in previous sections fix the design proposed of the IAXO optics. Different engineering drawings of the optics are shown in figure 12 and 13, where the 123 nested layers can be seen. Finally, its main design parameters are listed in table 2.

## 3.5 Final considerations

Our preliminary scoping study has made simplifying assumptions that will be revisited for the final design study.

- We have assumed the axion spectrum and intensity is uniformly emitted from a region 3 arcmin in extent. We must include the actual distributions in a full Monte Carlo model of the system performance.
- We have computed effective area for an on-axis point source. When the solar extent is included in ray-tracing, the area will decrease by a small amount.
- We have not accounted for non-specular scattering.



**Figure 11.** Value of the focal spot size  $\sqrt{a}$  (red squares and dashed line, right axis) and the figure of merit  $f_O$  (blue circles and solid line, left axis) versus focal length f. The optimal figure of merit is found for f = 5 m.

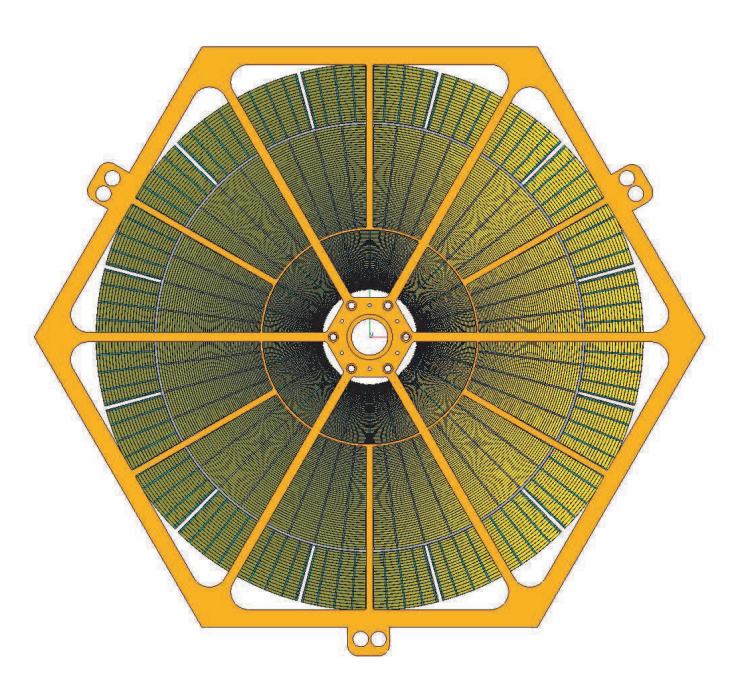


**Figure 12.** An edge-on view of one IAXO optic, including the hexagonal "spider" structure that will be used to mount the optic into the magnet bores. The thousands of individual mirror segments are visible.

- We have assumed the encircled energy function (EEF) evaluated at 50% (i.e., the half-power-diameter) is 1 arcminute and the EEF evaluated at 80% is 2 arcminute.
- $\bullet$  We have only coarsely studied how the focal length f influences the FOM in increments of 1 m.

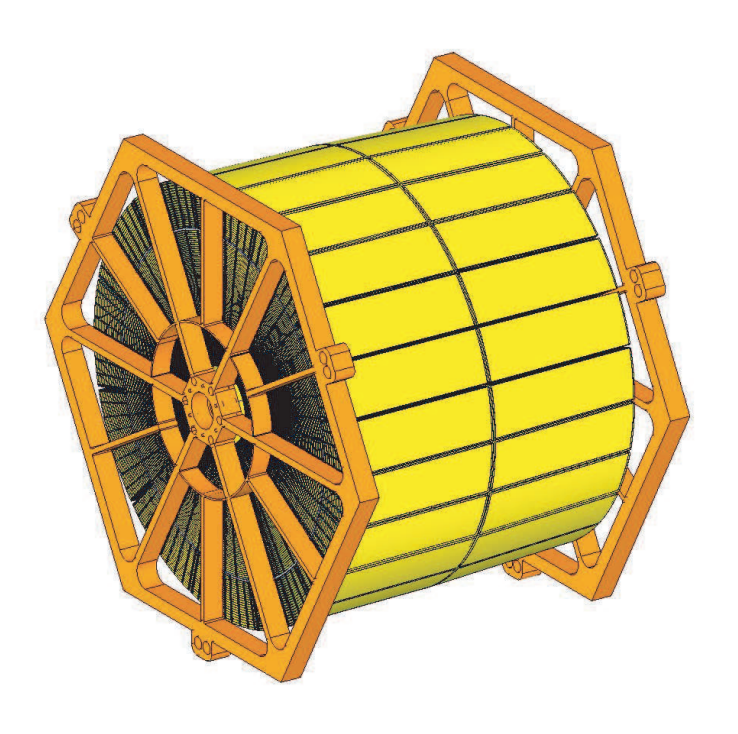


Figure 13. An isomorphic side-view of the telescopes and the spider mounting structures.

**Table 2.** Main design parameters of the IAXO x-ray telescopes.

Telescopes	8
N, Layers (or shells) per telescope	123
Segments per telescope	2172
Geometric area of glass per telescope	$0.38\mathrm{m}^2$
Focal length	5.0 m
Inner radius	50 mm
Outer Radius	300 mm
Minimum graze angle	2.63 mrad
Maximum graze angle	15.0 mrad
Coatings	W/B <sub>4</sub> C multilayers
Pass band	1-10 keV
IAXO Nominal, 50% EEF (HPD)	0.29 mrad
IAXO Enhanced, 50% EEF (HPD)	0.23 mrad
IAXO Nominal, 80% EEF	0.58 mrad
IAXO Enhanced, 90% EEF	0.58 mrad
FOV	2.9 mrad